THE JOURNAL OF PHYSICAL CHEMISTRY C

Article

pubs.acs.org/JPCC

Predicting New TiO_2 Phases with Low Band Gaps by a Multiobjective Global Optimization Approach

Hou-Zun Chen,† Yue-Yu Zhang,† Xingao Gong,* and Hongjun Xiang*

Key Laboratory of Computational Physical Sciences (Ministry of Education), State Key Laboratory of Surface Physics, and Department of Physics, Fudan University, Shanghai 200433, P. R. China

Supporting Information

ABSTRACT: TiO_2 has been extensively studied due to the possible application in solar cells and photoelectrochemical (PEC) water-splitting. However, the energy conversion efficiency is rather low because of the large band gaps (larger than 3.0 eV) of rutile and anatase TiO_2. Here we introduce the multiobjective differential evolution (MODE) method as a novel global optimization algorithm to predict new polymorphs of bulk TiO_2 with better optical properties than rutile and anatase TiO_2. The band gaps of the new PI (*Pnma*) and CI (C2) phases are found to be 1.95 and 2.64 eV. The calculation of formation energy, phonon dispersions, and thermal stability shows that the two novel phases are dynamically and thermally stable. These new TiO_2 polymorphs with better electronic and optical properties may pave a new way for high-efficiency solar energy conversion.

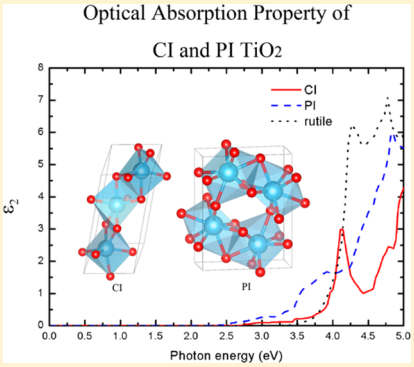

INTRODUCTION

Titanium dioxide (TiO_2) is a wide-gap semiconductor that can be widely used in applications from solar cells to photocatalyst and pigmentation.[1,2] In the past several decades, the tremendous amount of experimental and theoretical research has been performed in the field of semiconductor photocatalyst since Fushijima and Honda discovered the photoelectrochemistry (PEC) effect on anode TiO_2 in 1971.[3] TiO_2 was also used as the common photocathode in dye-sensitized solar cells.[4] For both water splitting and dye-sensitized solar cell applications, the optimal band gap for the oxide should be around 2.0 eV. However, the large band gap of TiO_2 (3.2 eV for the anatase phase and 3.0 eV for the rutile phase) leads to low absorption efficiency in the solar emission spectra. Different methods have been applied to narrow the gap of TiO_2 to make it suitable for sunlight absorption.[5−7] The most widely used approach is doping, but doping-induced charge carrier trapping and recombination sites could reduce the photochemical activity of TiO_2.[8] Therefore, a dopant-free TiO_2 phase with a suitable band gap is highly desirable.

In this article, we predict new metastable TiO_2 phases with low band gaps for the use as solar cells. To achieve this target, we propose a general multiobjective global optimization algorithm [i.e., multiobjective differential evolution (MODE)] for inverse design of materials. In this novel method, more than one objective function can be optimized simultaneously, for example, total energy, band gap, hardness, etc. Here, we are trying to search a TiO_2 phase that has better optical properties than rutile phase and is also relatively stable. This is equivalent to a global optimization problem of a biobjective function, i.e., total energy and band gap. By combining the MODE method with density functional calculations, we find numerous new metastable structures of TiO_2 with the band gap around 2.3 eV. In particular, the *Pnma* and C2 phases have band gaps of 1.95 and 2.64 eV, respectively. They are only 0.15 eV/atom and 0.11 eV/atom less stable than the rutile TiO_2, respectively.

METHODS

2.1. Multiobjective Differential Evolution (MODE) for Inverse Design. In the past two decades, great efforts have been made in crystal structure prediction, and various algorithms have been developed,[9−14] most of which only search for structures with the lowest total energy. In application, special properties such as light absorption, hardness, etc., are of great concern. Some methods take those properties into account while neglecting the total energy,[15,16] and it is possible that the structures found by those methods may have rather high energy.

Here, we developed a novel method for inverse design through applying multiobjective optimization methods to predict structures with respect to both total energy and properties, thus extending the crystal structure prediction problem from the single-objective domain to the multiobjective domain. For multiobjective problems, there is a set of optimal functions, so a Pareto front will be found, which is formed by several alternative optimal solutions in the search space. However, in traditional mathematical programming techniques,[17] the objectives are weighted and summed into a single goal, which do not consider all the objectives simultaneously and most of which find only a single optimal solution instead of

Received: November 20, 2013
Revised: January 9, 2014
Published: January 14, 2014

   dx.doi.org/10.1021/jp411437f | J. Phys. Chem. C 2014, 118, 2333−2337

the Pareto front. Here, the MODE algorithm we applied is a kind of evolutionary algorithm that inherently explores a set of possible solutions simultaneously enabling it to find the first Pareto front in the decision space.

In a multiobjective problem, the objective can be defined as

$$\min Z(x) = [z_1(x), z_2(x), ..., z_k(x)] \quad (1)$$

where x is the decision variable (the structural parameters in this study) in R^n and $z_i(x)$ is the objective function (total energy and band gap in this study). In most situations, because of the lack of information of the relationship between the objective functions, it is impossible to minimize all the k objectives simultaneously. Therefore, using evolutionary algorithms, we render to finding nondominated solutions in the search space to form a Pareto front in the decision space. Here the meaning of dominate is defined as follows: a vector $Z(x)$ is dominating another different vector $Z'(x)$, which is denoted as $Z(x) < Z(x')$, if and only if $z_i(x) \leq z_i(x')$ for all $i \in \{1,2,...,k\}$. A solution x is on the Pareto front if and only if there is no solution x' that satisfies $Z(x') < Z(x)$. All the nondominated solutions form the first Pareto front.

The MODE algorithm is a kind of multiobjective evolution algorithm that is widely used in real world applications.[18,19] Following the general procedure of differential evolution (DE) with a population of N_p, the algorithm is able to find a set of solutions on the first Pareto front. In MODE, there are three major operations: mutation, Pareto-based ranking, and selection, which are used iteratively to evolve the population.

The mutation operator is composed of two parts: differential vector and perturbation vector. For a dominated individual p_i, which is a vector of n variables, a quasi-best solution p_{best} is chosen randomly from the first Pareto front of the parent population. The differential vector is defined as the difference between p_i and p_{best}. If p_i is nondominated, the p_{best} will be itself and the differential vector vanishes. For each individual, a pair of solutions is chosen from the parent population to generate the perturbation vectors. Each element in a vector of the population will perform the following operation with the mutation probability C_r.

$$p'_i = \begin{cases} p_i + F(p_{r1} - p_{r2}) & \text{if } p_i \text{ is nondominated} \\ \gamma p_{best} + (1-\gamma)p_i + F(p_{r1} - p_{r2}) & \text{otherwise} \end{cases} \quad (2)$$

where p'_i is the offspring of p_i, γ and F are parameters in MODE, and $r_1, r_2 \in [1, N_p]$ are randomly selected and satisfy $r_1 \neq r_2 \neq i \neq$ best. The ranking scheme of the Pareto front is as follows:[20] sort all the solutions in the decision space and find those nondominated to form the first Pareto front. Remove the solution in the first Pareto front and sort the rest to find those nondominated to form the second Pareto front. Repeat the process until there is no solution in the search space. The selection operation is based on a greedy strategy: an offspring is placed into the population if and only if it dominates its main parent.[21]

In the crystal structure searching problem, an individual is defined as a vector of dimension $3N + 6$, which contains six lattice parameters that are three angles, three lattice vectors, and $3N$ atom coordinates of N atoms. A population with N_p structures is initialized considering the symmetry of the 230 space groups. In order to increase the efficiency, atomic coordinates and lattice parameters of the structures are locally optimized after initialization, which can reduce the noise in the complex searching space and simplify the task of finding the global minimum on the energy surface.[11] In order to design highly effective solar cell materials, total energy and a targeted direct band gap E_g^{opt} are set as fitness functions for minimization, so the objectives can be defined as

$$\min \text{fitness}_1 = \text{total energy}$$
$$\min \text{fitness}_2 = |E_g^{opt} - \text{direct gap}| + |\text{direct gap} - \text{indirect gap}| \quad (3)$$

In the equation of fitness$_2$, the first item is aimed at finding materials of which the direct band gap is closest to E_g^{opt}, and the second item is aimed at finding materials with direct gap. Ranking and selection of the individuals with respect to the objectives are performed. The structure on the first 60% Pareto fronts are kept for mutation, and the structure on the last 40% Pareto fronts are discarded and replaced by newly generated structures to keep the diversity of the population. After generating new structures by the mutation operation, we return to the local optimization step and continue the process until a predefined generation is reached. The complete procedure is shown in Figure 1.

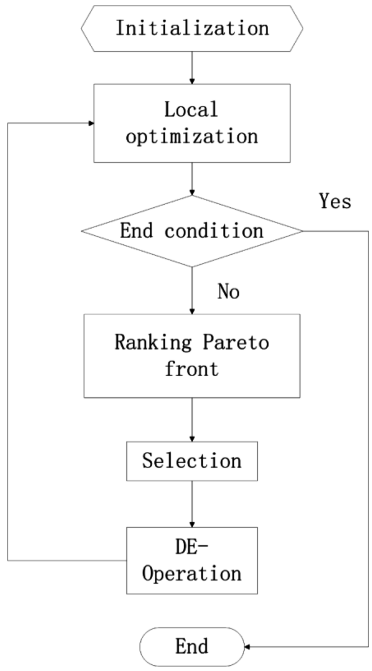

Figure 1. Procedure of the MODE algorithm. In the initialization step, crystal structures are generated with randomly selected space groups. Local optimization for each structure is performed after that. Then Pareto front ranking, selection, DE-operation, and local optimization are performed iteratively until the end condition (a predetermined generation) is reached.

In our calculation, the parameters in the mutation operation of MODE are set as $\gamma = 0.1$, $F = 0.2$, and $C_r = 1.0$ after performing careful tests. The population number is set as 30 and the generation number as 20.

2.2. DFT Calculations. In this work, we use density functional theory (DFT) method for structural relaxation and electronic structure calculation. The ion-electron interaction is treated by the projector augmented-wave (PAW) technique,[22] as implemented in the Vienna ab initio simulation package (VASP).[23] Moreover, the local-density approximation (LDA) is

dx.doi.org/10.1021/jp411437f | J. Phys. Chem. C 2014, 118, 2333−2337

adopted to calculate total energies and relax structures. In the MODE simulations, we also use LDA to estimate the band gaps of the specific structure to make the calculations affordable although LDA is well-known to underestimate the band gap. For the structures of the first Pareto front, the optical properties and accurate value of band gap are computed by employing the HSE06 functional, which was found to give accurate band gaps for semiconductors.[24] The 3D *k*-mesh is generated by the Monkhorst−Pack scheme, where the density of *k*-points is determined by lattice constant ($8 \times 12 \times 6$ for PI phase and $10 \times 10 \times 6$ for CI phase). Utilizing the direct method as implemented in the phonopy program,[14,25] the phonon calculations are performed to check the dynamic stability of a specific structure.

RESULTS AND DISCUSSION

3.1. Tests of the MODE Method. The DE algorithm has been proved to be an efficient method of cluster and grain boundary structure prediction.[26,27] To test the reliability of MODE method, bulk aluminum oxide (Al_2O_3) was chosen for the reason that there are multiple phases of Al_2O_3 with similar total energies but different band gaps. The specific value of 6.4 eV is set as an objective function of band gap and minimal total energy is set as the other. The code readily predicted that α-Al_2O_3 is expected to be the best structure of bulk aluminum oxide with a band gap of 6.4 eV within one or two generations. Another test focuses on the structures of carbon. If we set the targeted band gap as 4.1 eV, diamond structure can be found in an average of three steps. If the optimal band gap is altered to be 0.0 eV, graphene structure can be found in the same step as that in diamond.

3.2. Structures and Properties of the Predicted New Polymorphs of TiO_2. *3.2.1. Structure and Energy.* TiO_2 has many different polymorphs. Rutile, anatase, and brookite are the three most common polymorphs for TiO_2. Rutile is the most stable one if the size of TiO_2 crystal particle exceeds 35 nm.[28] In addition, another three metastable polymorphs of TiO_2 (monoclinic, tetragonal, and orthorhombic) at atmospheric pressure and five polymorphs [α-PbO_2-like (TiO_2II), baddeleyite-like (MI), cotunnite-like (OII), orthorhombic OI, cubic fluorite, and pyrite] at high pressure have been synthesized successfully.[29,30] From our systematic MODE simulations, hundreds of candidates of metastable polymorphs of TiO_2 were generated. The objective direct band gap E_g is set as 0.5 eV since LDA underestimates the band gap. Figure 2 shows the distribution of them by dots on the objective plane. The red dots highlight the Pareto front of our MODE search, which dominates all the other structures in this graph. From the Pareto front, we choose two structures based on the following criteria: (1) the band gap calculated by HSE06 is in the range (1.5, 3.0); (2) the structure is dynamically stable based on the phonon calculation; (3) thermal stability of the structure is confirmed by means of molecular dynamic simulations. These two structures with the *Pnma* and C_2 space groups are shown in Figure 3a,b. Hereafter, we refer to these two phases as PI and CI (Table 1). The LDA total energy of PI and CI is −9.53 and −9.57 eV/atom. For comparison, the LDA total energies of per atom of rutile TiO_2, fluorite-type TiO_2, and the pyrite-type TiO_2 are −9.68, −9.49, and −9.49 eV, respectively.[31] Therefore, these two phases are about 0.1 eV/atom less stable than rutile TiO_2 but are as stable as other TiO_2 phases. There are 4 Ti atoms and 8 O atoms in the unit cell of PI. Each Ti atom is 8-fold coordinated, and each O atom is 4-fold coordinated. There are 3 Ti atoms and 6 O atoms in the unit cell of CI. Each Ti atom is 6-fold coordinated, and each O atom is 3-fold coordinated, as in the cases of rutile and anatase.

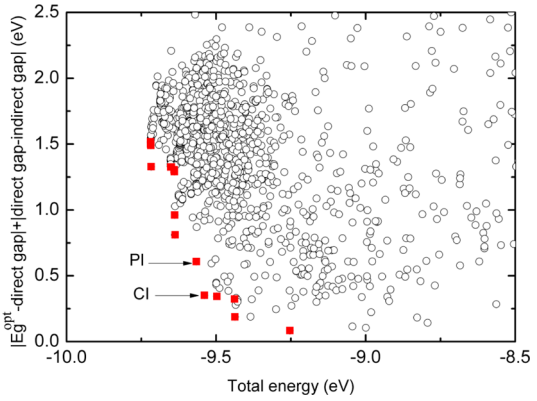

Figure 2. Distribution graph of objectives while optimizing total energy and band gap simultaneously. Each dot on the objective plane represents a structure generated by MODE algorithm. The objective functions are defined in eq 3. The dots marked by red color highlight the Pareto front of our MODE search, which dominates all of the rest of the dots in this graph. In this simulation, the target LDA band gap (E_g^{opt}) was set to be 0.5 eV.

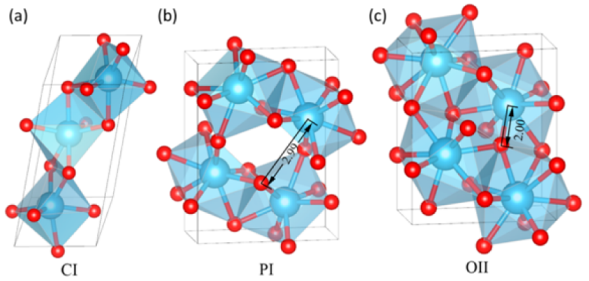

Figure 3. (a,b) Structure of CI and PI from the MODE simulations. The small red balls are O, while the Ti ions are located at the center of the light blue polyhedral. (b,c) Difference between PI and OII. The bond lengths denoted in the figure is in Å.

Table 1. Atomic Parameters for PI and CI[a]

		Wyckoff	*x*	*y*	*z*
PI	Ti1	4c	−0.3103	0.2500	0.3383
	O1	4c	0.3320	0.2500	0.4512
	O2	4c	0.0260	0.2500	−0.3092
CI	Ti1	2c	0.1971	0.4769	−0.1666
	Ti2	1b	0.0000	−0.3538	0.5000
	O1	2c	−0.4931	0.2880	−0.2618
	O2	2c	0.1718	0.3396	−0.4048
	O3	2c	0.1612	0.3089	0.0746

[a]The space group of PI is *Pnma* (No. 62) (lattice parameter a = 5.334 Å, b = 2.783 Å, and c = 6.788 Å). The space group of CI is *C*2 (No. 5) (lattice parameter a = 5.292 Å, b = 4.577 Å, c = 7.806 Å, $\alpha = \gamma = 90°$, and $\beta = 75°$).

3.2.2. Electronic Properties. It is well-known that the HSE06 functional predicts much better electronic properties than the LDA functional. For instance, the LDA gap of rutile TiO_2 is 1.73 eV, which is much smaller than the experimental band gap 3.30 eV.[32] In contrast, the band gap (3.18 eV) from the HSE06 calculation is much closer to the experimental value. Therefore, we perform our band structure calculations with the HSE06 functional. The band structures of the two new phases are

dx.doi.org/10.1021/jp411437f | J. Phys. Chem. C 2014, 118, 2333−2337

shown in Figure 4a,b. It is obvious that the CI has a direct band gap with $E_g \approx 2.64$ eV, while the PI is an indirect gap material

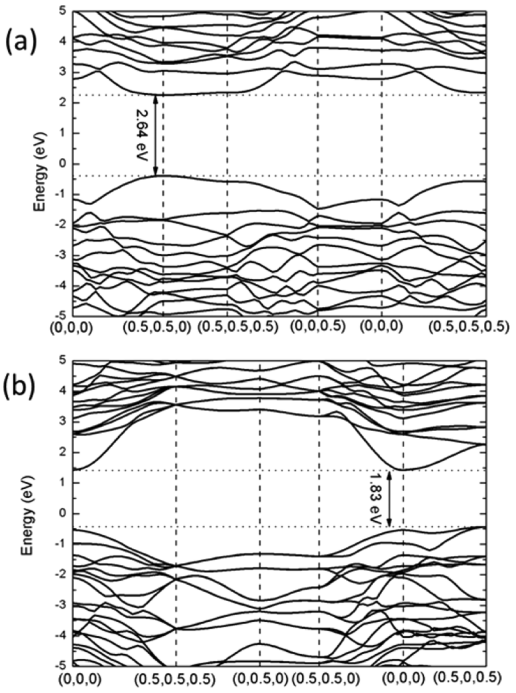

Figure 4. (a,b) HSE06 band structure of CI and PI. Both the VBM and CBM are denoted by dotted lines. The *k* points are shown by the fractional coordinates in the terms of the reciprocal lattice of the unit-cell. As we can see from the figure, the direct band gap (2.64 eV) of CI locates at (0.5, 0.5, 0). The VBM and CBM of PI appeared at (0.5, 0, 0.5) and (0, 0, 0), respectively. The direct gap is 1.95 eV, which is located at the gamma point.

with a direct gap of 1.95 eV and an indirect gap of 1.83 eV. We note that the structure of OII (one of the known polymorphs of TiO_2) with the same space group (*Pnma*) is similar to that of PI. The only structural difference (see Figure 3b,c) is that each Ti atom is 8-fold coordinated in PI but 9-fold coordinated in OII. The HSE06 band gap of OII is 3.01 eV, which is much larger than that (1.95 eV) of PI.

3.2.3. Optical Property. It is well-known that the imaginary part of the dielectric tensor $\varepsilon_2(\omega)$ determines the absorption ability of a material. Here we also adopt the HSE06 functional to compute $\varepsilon_2(\omega)$ accurately. Figure 5 shows the $\varepsilon_2(\omega)$ curves of the two new polymorphs with black and pink lines, respectively. For comparison, the corresponding results of rutile, anatase, brookite, OII, pyrite, and fluorite TiO_2 are also shown in the same figure. As we can see in Figure 5, the curves of CI and PI both rise before rutile and anatase, which indicate that PI and CI are better light absorbers than rutile and anatase. The curve of PI rises at about 2.5 eV; therefore, the absorption of PI can be extended to the visible region of the solar spectrum. The light absorption ability of PI is close to that of fluorite, which was also proposed to be a potential light absorber.[31] However, fluorite is not stable in standard ambient conditions because of the presence of imaginary frequencies in the phonon spectra, while PI and CI are dynamically stable. Furthermore, the PI and CI phases are found to be more stable than fluorite TiO_2 by −0.04 and −0.08 eV/atom, respectively.

As can be seen from Figure 5, CI TiO_2 starts to absorb light at an energy of the direct band gap (2.64 eV). This is because

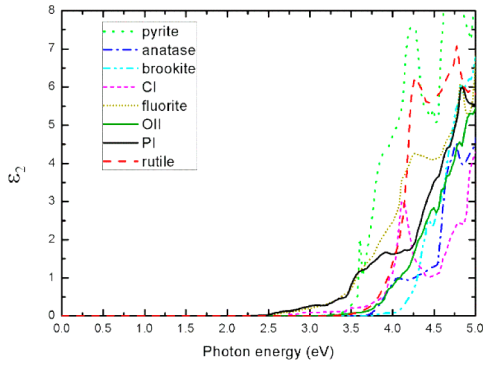

Figure 5. Imaginary part of dielectric functions of the two new TiO_2 polymorphs from the HSE06 calculations. For comparison, the imaginary part of dielectric functions of anatase, brookite, rutile, pyrite, fluorite, and OII from HSE06 is also shown.

all dipole transitions (including the direct band gap transition) in any system with a C_2 point group is allowed. However, PI TiO_2 starts to absorb light at 2.5 eV, which is larger than the electronic direct band gap (1.95 eV). We find that both VBM and CBM states at Γ have odd parity symmetry; thus, the direct band gap dipole transition is forbidden.

CONCLUSIONS

In summary, we developed a novel global optimization algorithm (i.e., multiobjective differential evolution (MODE)) to predict new material that possesses several desirable properties (for example, a low energy and a given band gap) simultaneously. By combining this method with first-principle calculations, we predict two new low band gap metastable TiO_2 phases (PI and CI) for solar energy applications. These two phases are found to have a better light absorption ability than other well-known TiO_2 polymorphs, and they are only slightly less stable (about 0.1 eV/atom) than rutile TiO_2. These news TiO_2 polymorphs are found to be both thermally and dynamically stable, which may be used in solar energy systems to improve the energy conversion efficiency. Furthermore, our MODE approach for inverse material design will pave a new way for predicting and designing other functional materials.

ASSOCIATED CONTENT

Supporting Information

Phonon dispersions and potential energies. This material is available free of charge via the Internet at http://pubs.acs.org.

AUTHOR INFORMATION

Corresponding Authors

*(X.G.) E-mail: xggong@fudan.edu.cn.
*(H.X.) E-mail: hxiang@fudan.edu.cn.

Author Contributions

†H.-Z.C. and Y.-Y.Z. contributed equally to this work.

Notes

The authors declare no competing financial interest.

ACKNOWLEDGMENTS

The authors thank Yang Zhou for completing part of the Inverse-Design of Materials by Multi-Objective Differential Evolution (IM^2ODE) package of structure searching and Hai-Yuan Cao for useful discussions. Work was supported by NSFC, the Special Funds for Major State Basic Research,

FANEDD, NCET-10-0351, Research Program of Shanghai Municipality and MOE, and Program for Professor of Special Appointment (Eastern Scholar).

REFERENCES

(1) Gao, H.; Li, X.; Lv, J.; Liu, G. Interfacial Charge Transfer and Enhanced Photocatalytic Mechanisms for the Hybrid Graphene/Anatase TiO_2(001) Nanocomposites. *J. Phys. Chem. C* **2013**, *117*, 16022−16027.
(2) Asahi, R.; Morikawa, T.; Ohwaki, T.; Aoki, K.; Taga, Y. Visible-Light Photocatalysis in Nitrogen-Doped Titanium Oxides. *Science* **2001**, *293*, 269−271.
(3) Fujishima, A.; Honda, K. Eletrohemical Photolysis of Water at a Semicinductor Electrode. *Nature* **1972**, *238*, 37−38.
(4) Bak, T.; Nowotny, J.; Rekas, M.; Sorrell, C. C. Photo-Electrochemical Properties of the TiO_2−Pt System in Aqueous Solutions. *Int. J. Hydrogen Energy* **2002**, *27*, 19−26.
(5) Tao, J.; Luttrell, T.; Batzill, M. A Two-Dimensional Phase of TiO_2 with a Reduced Bandgap. *Nat. Chem.* **2011**, *3*, 296−300.
(6) Khan, S. U. M.; Al-Shahry, M.; Ingler, W. B. Efficient Photochemical Water Splitting by a Chemically Modified *n*-TiO_2. *Science* **2002**, *297*, 2243−2245.
(7) Nikolay, T.; Larina, L.; Shevaleevskiy, O.; Ahn, B. T. Electronic Structure Study of Lightly Nb-Doped TiO_2 Electrode for Dye-Sensitized Solar Cells. *Energy Environ. Sci.* **2011**, *4*, 1480−1486.
(8) Choi, W.; Termin, A.; Hoffmann, M. R. The Role of Metal Ion Dopants in Quantum-Sized TiO_2: Correlation between Photoreactivity and Charge Carrier Recombination Dynamics. *J. Phys. Chem.* **1994**, *98*, 13669−13679.
(9) Pannetier, J.; Bassas-Alsina, J.; Rodriguez-Carvajal, J.; Caignaert, V. Prediction of Crystal Structures from Crystal Chemistry Rules by Simulated Annealing. *Nature* **1990**, *346*, 343−345.
(10) Wales, D. J.; Scheraga, H. A. Global Optimization of Clusters, Crystals, and Biomolecules. *Science* **1999**, *285*, 1368−1372.
(11) Oganov, A. R.; Glass, C. W. Crystal Structure Prediction Using Ab Initio Evolutionary Techniques: Principles and Applications. *J. Chem. Phys.* **2006**, *124*, 244704−244715.
(12) Pickard, C. J.; Needs, R. J. When is H_2O not Water? *J. Chem. Phys.* **2007**, *127*, 244503−244507.
(13) Wang, Y.; Lv, J.; Zhu, L.; Ma, Y. Crystal Structure Prediction via Particle-Swarm Optimization. *Phys. Rev. B* **2010**, *82*, 094116.
(14) Luo, X.; Yang, J.; Liu, H.; Wu, X.; Wang, Y.; Ma, Y.; Wei, S.-H.; Gong, X.; Xiang, H. Predicting Two-Dimensional Boron−Carbon Compounds by the Global Optimization Method. *J. Am. Chem. Soc.* **2011**, *133*, 16285−16290.
(15) Xiang, H. J.; Huang, B.; Kan, E.; Wei, S.-H.; Gong, X. G. Towards Direct-Gap Silicon Phases by the Inverse Band Structure Design Approach. *Phys. Rev. Lett.* **2013**, *110*, 118702−118706.
(16) Zhang, X.; Wang, Y.; Lv, J.; Zhu, C.; Li, Q.; Zhang, M.; Li, Q.; Ma, Y. First-Principles Structural Design of Superhard Materials. *J. Chem. Phys.* **2013**, *138*, 114101−114109.
(17) Eckenrode, R. T. Weighting Mltiple Criteria. *Operations Research* **1962**, *10*, 27−27.
(18) Xue, F.; Sanderson, A. C.; Graves, R. J. Pareto-Based Multi-Objective Differential Evolution. In *The 2003 Congress on Evolutionary Computation, CEC '03*, Dec. 8−12 2003; IEEE: New York, 2003; Vol. *2*, pp 862−869.
(19) Robič, T.; Filipič, B. DEMO: Differential Evolution for Multiobjective Optimization. In *Evolutionary Multi-Criterion Optimization*; Springer: Berlin, Germany, 2005; Vol. *3410*, pp 520−533.
(20) Deb, K.; Pratap, A.; Agarwal, S.; Meyarivan, T. A Fast and Elitist Multiobjective Genetic Algorithm: NSGA-II. Evolutionary Computation. *IEEE Trans.* **2002**, *6*, 182−197.
(21) Abbass, H. A.; Sarker, R.; Newton, C. In PDE: a Pareto-frontier Differential Evolution Approach for Multi-objective Optimization Problems. In *Proceedings of the 2001 Congress on Evolutionary Computation*; IEEE: New York, 2001; Vol. *2*, pp 971−978.
(22) Blöchl, P. E. Projector Augmented-Wave Method. *Phys. Rev. B* **1994**, *50*, 17953−17979.
(23) Kresse, G.; Hafner, J. Ab Initio Molecular-Dynamics Simulation of the Liquid-Metal−Amorphous-Semiconductor Transition in Germanium. *Phys. Rev. B* **1994**, *49*, 14251−14269.
(24) Heyd, J.; Scuseria, G. E.; Ernzerhof, M. Hybrid Functionals Based on a Screened Coulomb Potential. *J. Chem. Phys.* **2003**, *118*, 8207−8215.
(25) Togo, A.; Oba, F.; Tanaka, I. First-Principles Calculations of the Ferroelastic Transition between Rutile-Type and $CaCl_2$-Type SiO_2 at High Pressures. *Phys. Rev. B* **2008**, *78*, 134106−134115.
(26) Chen, Z.; Jiang, X.; Li, J.; Li, S.; Wang, L. PDECO: Parallel Differential Evolution for Clusters Optimization. *J. Comput. Chem.* **2013**, *34*, 1046−1059.
(27) Li, Z.-L.; Cao, H.-Y.; Yang, J.-H.; Shu, Q.; Zhang, Y.-Y.; Xiang, H.; Gong, X. What Is Armchair-Zigzag Grain Boundary Structure in Graphene? *arXiv:1308.3964*, 2013.
(28) Zhang, H. Z.; Banfield, J. F. Understanding Polymorphic Phase Transformation Behavior During Growth of Nanocrystalline Aggregates: Insights from TiO_2. *J. Phys. Chem. B* **2000**, *104*, 3481−3487.
(29) Mattesini, M.; de Almeida, J. S.; Dubrovinsky, L.; Dubrovinskaia, N.; Johansson, B.; Ahuja, R. High-Pressure and High-Temperature Synthesis of the Cubic TiO_2 Polymorph. *Phys. Rev. B* **2004**, *70*, 212101−212105.
(30) Dubrovinsky, L. S.; Dubrovinskaia, N. A.; Swamy, V.; Muscat, J.; Harrison, N. M.; Ahuja, R.; Holm, B.; Johansson, B. Materials Science: The Hardest Known Oxide. *Nature* **2001**, *410*, 653−654.
(31) Mattesini, M.; de Almeida, J. S.; Dubrovinsky, L.; Dubrovinskaia, N.; Johansson, B.; Ahuja, R. Cubic TiO_2 As a Potential Light Absorber in Solar-Energy Conversion. *Phys. Rev. B* **2004**, *70*, 115101−115110.
(32) Tezuka, Y.; Shin, S.; Ishii, T.; Ejima, T.; Suzuki, S.; Sato, S. Photoemission and Bremsstrahlung Isochromat Spectroscopy Studies of TiO_2 (Rutile) and $SrTiO_3$. *J. Phys. Soc. Jpn.* **1994**, *63*, 347−357.